Muxworthy, A R, Roberts, A P, **First-order reversal curve (FORC) diagrams**, In: Gubbins, D and Herrero-Bervera, E, editor, Encyclopedia of Geomagnetism and Paleomagnetism, Springer, 2007, Pages: 266 - 272

FIRST-ORDER REVERSAL CURVE (FORC) DIAGRAMS

Adrian R. Muxworthy* and Andrew P. Roberts

School of Ocean and Earth Science, National Oceanography Centre, European Way,

University of Southampton, Southampton, SO14 3ZH, UK.

*Corresponding author:

Tel: +44 (0) 23 8056573 Fax: +44 (0) 23 80593059

Email: adrian.muxworthy@soton.ac.uk

Outline:

FIRST-ORDER REVERSAL CURVE (FORC) DIAGRAMS

Introduction

In many geomagnetic, geological and environmental magnetic studies, it is important to have reliable methods of characterizing the composition and grain size distribution of magnetic minerals within samples. For example, identification of single domain (SD) magnetic grains is important in absolute paleointensity studies because SD grains produce the most reliable results, while larger multi-domain (MD) grains yield the least meaningful results. In paleoclimatic studies, useful environmental information is often revealed by subtle changes in grain size distribution, as revealed by domain state, while the same grain size variations will complicate determination of relative paleointensity from the same sediment. It is therefore crucially important to have reliable methods for determining the magnetic grain size distribution in a wide range of geomagnetic, paleomagnetic and environmental magnetic applications.

Determining the composition of magnetic minerals in a rock is relatively straightforward; however, identification of the domain state is more difficult. Conventional methods, such as measurement of magnetic hysteresis, can be powerful, but they can also yield ambiguous results because various combinations of mineral composition, grain size, internal stress and magnetic interactions among the grains can produce the same magnetic behaviour. This is particularly true for the commonly used Day plot (Day *et al*. 1977), which summarizes the bulk magnetic hysteresis properties by plotting ratios of M_{rs}/M_s versus H_{cr}/H_c, where M_{rs} is the saturation remanent magnetization, M_s is the saturation magnetization, H_{cr} is the coercivity of remanence, and H_c is the coercive force (see **Hysteresis** for a description of how these parameters are determined). For example, numerical studies have shown that magnetostatic interactions among ideal SD grains can cause the bulk hysteresis parameters of samples to plot within the MD region of the Day plot (Muxworthy *et al*. 2003).

In an attempt to remove some of the ambiguity inherent to conventional hysteresis measurements, Pike *et al*. (1999) and Roberts *et al.* (2000) developed a method of mineral and domain state discrimination using a type of hysteresis curve called a first-order reversal curve (FORC). Measurement of a suite of FORCs provides detailed information from within the major hysteresis loop, which enables determination of the distribution of switching fields and interaction fields for all of the particles that contribute to the hysteresis loop. The ability to measure sufficient FORCs to construct a FORC diagram has only recently become possible with rapid and sensitive vibrating sample magnetometers and alternating gradient magnetometers.

Measuring and constructing FORC diagrams

A FORC is measured by progressively saturating a sample in a field H_{SAT}, decreasing the field to a value H_A, reversing the field and sweeping it back to H_{SAT} in a series of regular field steps (H_B) (Fig. 1a). This process is repeated for many values of H_A, which yields a series of FORCs, and the measured magnetization M at each step as a function of H_A and H_B gives $M(H_A, H_B)$ (Fig. 1b). $M(H_A, H_B)$ can then be plotted as a function of H_A and H_B in field space (Fig. 1c). The field steps are chosen such that H_A and H_B are regularly spaced, which means that $M(H_A, H_B)$ can be plotted on a regular grid. The FORC distribution $\rho(H_A, H_B)$ is defined as the mixed second derivative of the surface shown in Fig. 1c:

$$\rho(H_A, H_B) \equiv -\partial^2 M(H_A, H_B) / \partial H_A \partial H_B. \quad (1)$$

When $\rho(H_A, H_B)$ is plotted as a contour plot (i.e., as a FORC diagram; Fig. 1d), it is convenient to rotate the axes by changing coordinates from (H_A, H_B) to $H_C = (H_B - H_A)/2$ and $H_U = (H_B + H_A)/2$.

As is standard when fitting functions to experimental data, reduction of the effect of noise on FORC distributions is achieved in a piece-wise manner. That is, rather than fitting a function to the entire $M(H_A, H_B)$ surface and then directly differentiating this surface to determine $\rho(H_A, H_B)$, the FORC distribution is determined at each point by fitting a mixed second-order polynomial of the form $a_1 + a_2H_A + a_3H_A^2 + a_4H_B + a_5H_B^2 + a_6H_AH_B$ to a local, moving grid. $\rho(H_A, H_B)$ is simply equal to the fitted parameter $-a_6$. As the polynomial is only of second order, it cannot accurately accommodate complex surfaces; however, this will not commonly be a problem for geological or environmental samples, which usually have relatively smooth FORC distributions. The size of the local area is determined by a user-defined smoothing factor (SF), where the size of the grid is simply $(2SF+1)^2$. SF normally takes values between 2 and 5, although ideally it should be 2. Taking the second derivative in equation (1) magnifies the noise that is inevitably present in the magnetization data. Increasing SF reduces the contribution of noise to the resulting FORC diagram, but it also removes measured data. Simple tests can be conducted to determine suitable smoothing factors for each sample. These tests determine when all of the noise that has been removed by smoothing; if SF is increased above this value, the effect will be only to remove data (Heslop and Muxworthy, 2005).

A FORC diagram is well described by 100-140 raw FORCs. Recent improvements in system hardware have made it possible to measure 100 FORCs in approximately 1 hour. The exact time depends on the field-step size, the aspect ratio of the FORC diagram, H_{SAT} and the averaging time. The effects of these measurement variables depend as follows.

(1) The chosen field-step size depends ultimately on the mineralogy of the sample under investigation. For a simple SD-dominated sample as in Fig. 1d, the main peak of the FORC diagram is directly related to the coercive force H_c. It is necessary to choose suitable boundary values for H_U and H_C to fully depict the FORC distribution. The field-step size will be larger for FORC diagrams with larger boundary values, which then increases the measurement time. That is, it will take longer to measure a FORC diagram dominated by high coercivity minerals such as hematite compared to low coercivity minerals such as magnetite.

(2) The aspect ratio of the FORC diagram also affects the measurement time. The overall measurement time will decrease as the ratio of the length of the axes, i.e., (H_U axis)/(H_C axis), increases. A square FORC diagram therefore is optimal in terms of measurement time (but the characteristics of the measured sample should dictate the selected axis lengths). Also, in order to rigorously calculate a FORC distribution, it is necessary to measure points outside the limits of the FORC diagram (depending on the value of SF). This will also (marginally) increase the measurement time.

(3) H_{SAT} should be sufficient to magnetically saturate the sample. However, making H_{SAT} unnecessarily large will increase measurement time because of the finite time taken to sweep the magnet down from high values of H_{SAT}.

(4) The averaging time is the amount of time taken to measure each data point, and is usually 0.1 - 0.25 seconds (s). Typically, the averaging time is set to 0.15 s. Increasing the averaging time increases the total measurement time, but improves signal to noise ratios. In systems that magnetically relax on the same time scale as the averaging time, the averaging time can be critical to the resulting FORC diagram. The averaging time should therefore always be stated in the accompanying text or figure caption.

FORC and Preisach diagrams

The FORC method originates in the phenomenological Preisach-Néel theory of hysteresis (Preisach, 1935; Néel, 1954). There has been much unnecessary confusion in the paleomagnetic community over the relationship between Preisach diagrams and FORC diagrams. Much of this confusion has arisen due to the lack of understanding as to what a Preisach diagram is. Put simply, there a many ways of measuring a Preisach diagram, of which the FORC method is one.

FORC diagrams are essentially a new well-defined algorithm or method for rapidly generating a particular class of Preisach diagram.

Characteristic FORC diagrams

Non-interacting SD behaviour

To help in the understanding of FORC diagrams, consider a FORC diagram for a SD grain, with uniaxial anisotropy, that is aligned in the direction of the applied field. Such an ideal SD grain will have a perfect square hysteresis loop (Fig. 2a). When plotting raw FORC data for such a particle in non-rotated field space, $M(H_A, H_B)$ can take one of two values, i.e., $+M_s$ or $-M_s$ (Fig. 2b). For $H_A > -H_{SW}$ (where H_{SW} is the switching field), $M(H_A, H_B)$ is $+M_s$, for $H_A < -H_{SW}$ and $H_B < +H_{SW}$, $M(H_A, H_B)$ is $-M_s$, and for $H_A < -H_{SW}$ and $H_B > +H_{SW}$, $M(H_A, H_B)$ is $+M_s$. On differentiating the surface with respect to H_A and H_B, only at $H_A = H_B = H_{SW}$ is $M(H_A, H_B)$ non-zero. That is, the FORC distribution should be a perfect delta function, normal to the FORC plane; however, due to the smoothing factor, $\rho(H_A, H_B)$ will have finite width (Fig. 2c). An ideal non-interacting uniaxial SD particle with field applied along the easy axis of magnetization will therefore have a FORC distribution that lies at $H_c = H_{SW}$ and $H_u = 0$.

For assemblages of randomly orientated, non-interacting, identical, uniaxial SD grains, there are three main features in the FORC diagram (Fig. 3): first, there is a central peak; second, the main peak displays an asymmetric "boomerang" shape; and third, there is a negative region near the bottom left-hand corner of the FORC diagram. The central peak is due to the switching of the magnetization at H_{SW}. From a more mathematical point of view, the positive peak is associated with the increase in $\partial M/\partial H_B$ with decreasing H_A as highlighted in Fig. 3. The lower left-hand arm of the boomerang is related to FORCs near the relatively abrupt positive switching field. The right-hand arm of the boomerang is related to more subtle contours, which are due to the FORCs having different return paths, as highlighted in Fig. 3. The shape of the return paths is controlled by the orientation of the grains with respect to the applied field, which results from the fact that the orientation controls the coercivity. Initially, return curve behaviour is dominated by grains oriented ~45° to the field. As H_A decreases, grains with orientations closer to 90° and 0° will start contributing to the hysteresis curve, so each time H_A is decreased the return path includes grains with slightly differently shaped hysteresis loops. The right-hand arm is therefore a result of moving from the return path for a 45° assemblage in the first instance, into the return path for a randomly orientated assemblage. This effect is particularly enhanced for an assemblage of identical grains. The origin of the negative region is related to sections of the

FORCs where $H_B < 0$ (Newell, 2005). As illustrated in Fig. 3, $\partial M/\partial H_B$ decreases with decreasing H_A at H_{B_1}, which gives rise to negative values for $\rho(H_A, H_B)$. The decrease in $\partial M/\partial H_B$ with H_A is not as pronounced for $H_B < 0$; consequently the negative region is significantly smaller than the large central peak near H_{B_2}. If the SD grains have a distribution of switching fields, this causes the FORC diagram to stretch out in the H_C direction (Fig. 4). A distribution of coercivities (e.g., Fig. 4) is much more typical of natural samples than an assemblage of identical grains as depicted in Fig. 3.

Interacting SD behaviour

FORC distributions are highly sensitive to magnetostatic interactions. As a starting point to understanding the contribution of interactions to the FORC diagram, it is simplest to consider Néel's (1954) interpretation of the Preisach (1935) diagram. Néel (1954) showed that for interacting SD grains, H_C corresponds to the coercive force of each SD loop in the absence of interactions and that H_U is the local interaction field H_I. It follows in the Preisach-Néel interpretation that $\rho(H_a, H_b)$ is the product of two distributions: the coercivity distribution $g(H_C)$ and the interaction field distribution $f(H_U)$. In a simple visualization, when the ideal SD grain in Fig. 2a is affected by magnetic interactions, H_I will shift the switching field (Fig. 5a). This asymmetry between the forward and backward switching fields gives rise to spreading in the H_U direction on a FORC diagram (Fig. 5b). Micromagnetic models for FORC diagrams have shown that Néel's (1954) approximation is correct for moderately interacting systems, but that it breaks down when the grains are separated by less than a grain width (Muxworthy *et al*. 2004). Highly interacting systems produce FORC diagrams that appear to be essentially the same as those for MD grains (see below and compare Fig. 5 with Pike *et al*. 2001a).

MD and pseudo-single domain grains

FORC diagrams for large MD grains (Pike *et al*. 2001a) produce a series of contours that run parallel or nearly parallel to the H_U axis (Fig. 6a). This spreading of the FORC distribution is essentially the same as for interacting SD grains; instead of the spreading being due to inter-grain magnetostatic interaction fields, it is due to internal demagnetizing fields. Pseudo-single domain (PSD) grains display behaviour intermediate between true MD and true SD behaviour (Fig. 6b). That is, they display both the closed peak structures observed for SD grains and the more open contours that become increasingly parallel to the H_U axis with coarser grain sizes (Roberts *et al*. 2000).

Superparamagnetic behaviour

Superparamagnetic (SP) grains will only manifest themselves on the FORC diagram if their relaxation time is of the same order as the averaging time (Roberts *et al*. 2000; Pike *et al*. 2001b). If the grains have shorter relaxation times, i.e., $H_{SW} \rightarrow 0$, then $\rho(H_A, H_B) = 0$ at all values. SP grains with relaxation times of ~0.1-0.25 s have FORC diagrams similar to those for MD grains, i.e., $\rho(H_A, H_B)$ plots as a series of contours running almost parallel to the H_U axis (Fig. 6c). Although SP behaviour may initially seem similar to MD behaviour, the coercivity spectra of MD and SP samples and the shapes of the FORC distributions can be visually distinguished (Fig. 6a, c). Cooling a sample by a few degrees can also easily enable identification of thermal relaxation. Due to the exponential nature of SD relaxation times, small temperature variations are sufficient to increase relaxation times, which effectively makes the grains thermally stable on the time scale of a measurement. Upon cooling, the FORC diagram for a SP sample would then resemble that of a stable SD sample (cf. Fig. 4). In contrast, FORC diagrams for MD samples would not display such variations with temperature.

Further Features of FORC diagrams

The H_U axis

Due to the use of the local grid when calculating a FORC diagram for any value of SF, it is necessary to fit the polynomial surface using points outside the plotted FORC diagram. For the upper, lower and right-hand bounds of the FORC diagram, this is readily achievable by simply measuring extra data points. For the H_U axis, however, this is not possible. This means that points on the H_U axis are not directly measured, and there will be a gap of size 2SF+1 multiplied by the field spacing between $\rho(H_A, H_B)$ and the H_U axis on the FORC diagram. Three approaches have been made to deal with this problem.

(1) Do not plot the FORC distribution for the region where the polynomial cannot be rigorously calculated. This results in a "truncated" FORC diagram (Fig. 7a).

(2) Relax the calculation of $\rho(H_A, H_B)$ back on to the H_U axis by reducing the smoothing near the H_U axis. Such "relaxed fit" diagrams (Fig. 7b) will produce distortions, which can give misleading results if the field step size is too large, but they have the advantage that it is at least possible to observe low coercivity magnetization components. Such components are usually

important in natural samples, so relaxing the fit is considered by some workers to be preferable to truncation.

(3) Reversible-ridge method (Fig. 7c) (Pike, 2003). This approach, which has been developed from Preisach theory, accommodates the reversible component of the magnetization data in addition to the irreversible part. With this approach, FORCs are extrapolated beyond $H_A < 0$, which enables rigorous calculation of $\rho(H_A, H_B)$ back on to the H_U axis. For SD assemblages this approach can be successful, however, for natural samples containing PSD or MD material the reversible ridge can often swamp the signal from the irreversible component of magnetization.

Asymmetry of FORC diagrams

The FORC method is a highly asymmetric method of measuring a Preisach diagram. The asymmetry originates from the measurement method in which each FORC starts from a saturated state. In interacting SD and MD systems, this means that there is bias in the magnetostatic interaction and internal demagnetizing fields in the direction of H_{SAT}. The only FORCs that do not contain a history of the initial H_{SAT} state are those that start from a sufficiently large negative H_A value that saturates the sample in the opposite direction. Asymmetry is therefore inherent to FORC diagrams.

Applications of the FORC diagram

FORC diagrams provide much more detailed information about magnetic assemblages than standard hysteresis measurements. Thermal relaxation, variations in domain state and magnetostatic interactions all produce characteristic and distinct manifestations on a FORC diagram. Here we illustrate four applications of FORC diagrams in paleomagnetic and environmental magnetic studies.

(1) *Unravelling mixed magnetic assemblages*. A key problem in many paleomagnetic and environmental studies is identifying and isolating specific minerals and/or grain size distributions within a sample. This can be difficult in mixed samples if the signal from one mineral is magnetically swamped by that of another mineral. FORC diagrams have been shown to be successful at identifying magnetic signals due to minerals with low intrinsic magnetizations when they are present along with more strongly magnetic minerals (Roberts *et al*. 2000; Muxworthy *et al*. 2005). For example, consider a mixture of PSD magnetite and PSD hematite.

The hysteresis loop in Fig. 8a provides no evidence for the presence of hematite, whereas in the FORC diagram the presence of hematite is clearly visible by the high-coercivity component that extends to high values of H_C (Fig. 8b). Although the FORC diagram is more successful than standard magnetic hysteresis measurements at identifying weaker magnetic phases in mixtures with more strongly magnetic phases, there are still concentration thresholds beyond which the magnetic signal of the strongly magnetic phase dominates and the weakly magnetic phase is no longer detectable in FORC diagrams (Muxworthy *et al*. 2005). In such cases, other magnetic methods may be more suitable than FORC analysis. For example, in mixtures of MD magnetite and hematite, low-temperature techniques can be more sensitive than FORC diagrams at identifying hematite in the presence of magnetite.

(2) *Source discrimination*. Due to the detailed nature of FORC diagrams, they can be used to identify subtle differences between source materials that are not so readily observed using magnetic hysteresis data. For example, in a study of a loess/paleosol sequence from Moravia, two different source materials could be clearly distinguished and identified using FORC diagrams (van Oorschot *et al*. 2002). There are many other apparent uses of FORC diagrams in environmental magnetic applications.

(3) *Assessing leaching*. Sequential leaching techniques are commonly used by soil chemists to remove iron oxides from samples to facilitate clay mineral analysis. FORC analysis has been shown to help in elucidation of the leaching process where magnetic hysteresis alone was less diagnostic (Roberts *et al*. 2000).

(4) *Pre-selection for paleointensity studies*. In absolute paleointensity studies, SD assemblages should provide reliable results, while samples with strong magnetostatic interactions and/or MD grains should yield unacceptable results. Domain state and magnetostatic interactions are both readily identifiable on a FORC diagram, which should make them useful for sample screening and selection for absolute paleointensity studies. Likewise, strict criteria apply to the mineralogy, domain state and concentration of magnetic particles in sedimentary sequences in terms of their suitability for relative paleointensity studies. FORC diagrams therefore also have potential for screening sediments for relative paleointensity studies.

Bibliography

Day, R., Fuller, M. and Schmidt, V. A., 1977. Hysteresis properties of titanomagnetites: grain-size and compositional dependence. *Physics of the Earth and Planetary Interiors*, 13, 260-267.

Heslop, D. and Muxworthy, A. R., 2005. Aspects of calculating first-order-reversal-curve distributions. *Journal of Magnetism and Magnetic Materials*, 288, 155-167.

Muxworthy, A. R., Heslop, D. and Williams, W., 2004. Influence of magnetostatic interactions on first-order-reversal-curve (FORC) diagrams: a micromagnetic approach. *Geophysical Journal International*, 158, 888-897.

Muxworthy, A. R., King, J. G. and Heslop, D., 2005. Assessing the ability of first-order reversal curve (FORC) diagrams to unravel complex magnetic signals, *Journal of Geophysical Research*, 110, B01105, doi:10.1029/2004JB003195.

Muxworthy, A.R., Williams, W., and Virdee, D., 2003. Effect of magnetostatic interactions on the hysteresis parameters of single-domain and pseudo-single domain grains, *Journal of Geophysical Research*, 108, B11, 2517, doi:10.1029/2003JB002588.

Néel, L., 1954. Remarques sur la théorie des propriétés magnétiques des substances dures. *Applied Scientific Research B*, 4, 13-24.

Newell, A. J., 2005. A high-precision model of first-order reversal curve (FORC) functions for single-domain ferromagnets with uniaxial anisotropy. *Geochemistry, Geophysics, Geosystems*, 6, Q05010, doi:10.1029/2004GC000877.

Pike, C. R., 2003. First-order reversal-curve diagrams and reversible magnetization. *Physics Review B*, 104424.

Pike, C. R., Roberts, A. P. and Verosub, K. L., 1999. Characterizing interactions in fine magnetic particle systems using first order reversal curves. *Journal of Applied Physics,* 85, 6660-6667.

Pike, C. R., Roberts, A. P., Dekkers, M. J. and Verosub, K. L., 2001a. An investigation of multi-domain hysteresis mechanisms using FORC diagrams, *Physics of the Earth and Planetary Interiors,* 126, 13-28.

Pike, C. R., Roberts, A. P. and Verosub, K. L., 2001b. First-order reversal curve diagrams and thermal relaxation effects in magnetic particles, *Geophysical Journal International*, 145, 721-730.

Preisach, F., 1935. Über die magnetische Nachwirkung. *Zeitschrift für Physik*, 94, 277-302.

Roberts, A. P., Pike, C. R. and Verosub, K. L., 2000. First-order reversal curve diagrams: a new tool for characterizing the magnetic properties of natural samples. *Journal of Geophysical Research*, 105, 28461-28475.

van Oorschot, I. H. M., Dekkers, M. J. and Havlicek, P., 2002. Selective dissolution of magnetic iron oxides with the acid- ammonium-oxalate/ferrous-iron extraction technique - II. Natural loess and palaeosol samples. *Geophysical Journal International*, 149, 106-117.

Cross references

Hysteresis

Figure captions

Figure 1. Illustration of how FORC diagrams are constructed. (a) After applying a field at positive saturation (H_{SAT}), the field is reversed to H_A and is then progressively increased at a range of H_B values in the direction of H_{SAT}. The magnetization is denoted by $M(H_A, H_B)$. The dashed line represents the major hysteresis loop and the solid line represents a single FORC. (b) A set of consecutive FORCs. (c) The $M(H_A, H_B)$ surface plotted in non-rotated field space (H_A, H_B). (d) The resulting FORC diagram for the data shown in (b) and (c) for SF = 4. The FORC data shown in (b) to (d) are for a numerical model of randomly orientated uniaxial SD grains.

Figure 2. (a) Schematic square hysteresis loop for an ideal non-interacting SD particle, with uniaxial anisotropy, aligned along the direction of the applied field (H_{SW} is the switching field). (b) The raw hysteresis data for a series of FORCs for the grain shown in (a) plotted in non-rotated field space (H_A, H_B). (c) FORC diagram for data shown in (a) and (b). The FORC distribution for this grain lies at $H_c = H_{SW}$ and $H_u = 0$.

Figure 3. FORCs and FORC diagram for a numerical model of non-interacting 1000 identical SD grains with randomly distributed uniaxial anisotropy (modified after Muxworthy *et al.* (2004). The origins of the negative and positive regions in the FORC diagram are highlighted (SF = 4). The negative region is due to a decrease in $\partial M/\partial H_B$ with decreasing H_A for negative values of H_B (H_{B_1}). The large positive peak is associated with the increase in $\partial M/\partial H_B$ with decreasing H_A for positive values of H_B, near the switching field (H_{B_2}). The different return paths give rise the to the positive region of the FORC distribution to the right of the main peak as illustrated.

Figure 4. FORC diagram (SF = 3; averaging time = 0.15 s) for an assemblage of non-interacting ideal SD grains for a tuff sample from Yucca Mountain, Nevada (from Roberts *et al.* (2000).

Figure 5. (a) Schematic diagram depicting the effect of a local interaction field H_I on a square hysteresis loop for an ideal SD particle, with uniaxial anisotropy, aligned along the direction of the applied field, as shown in Fig. 2a. (b) Numerical simulation for an assemblage of 1000 evenly-spaced, magnetite-like ideal SD grains with oriented uniaxial anisotropy. The distance between grains is 1.5 times the grains size.

Figure 6. (a) FORC diagram (SF = 4; averaging time = 0.2 s) for a MD magnetite sample (mean grain size of 76 μm). (b) FORC diagram (SF = 3; averaging time = 0.15 s) for a PSD magnetite sample (mean grain size of 1.7 μm). (c) FORC diagram (SF = 3; averaging time =

0.2 s) for tuff sample CS014 from Yucca Mountain, Nevada, containing SP magnetite (from Roberts *et al.* (2000).

Figure 7. Illustration of three methods for fitting a FORC diagram. (a) A "truncated" FORC diagram, with no extrapolation of data onto the H_U axis; (b) a "relaxed-fit" FORC diagram with extrapolation onto the H_U axis; and (c) "reversible-ridge" fitting (following Pike, 2003). The sample is a PSD magnetite (mean grain size of 0.3 μm; SF = 4; averaging time = 0.1s).

Figure 8. (a) Major hysteresis loop and (b) FORC diagram for a sample containing PSD magnetite and PSD hematite in a ratio of 81:19. On the FORC diagram, the hematite is readily identified, but it is not evident in the major hysteresis loop (SF = 3; averaging time = 0.15 s).

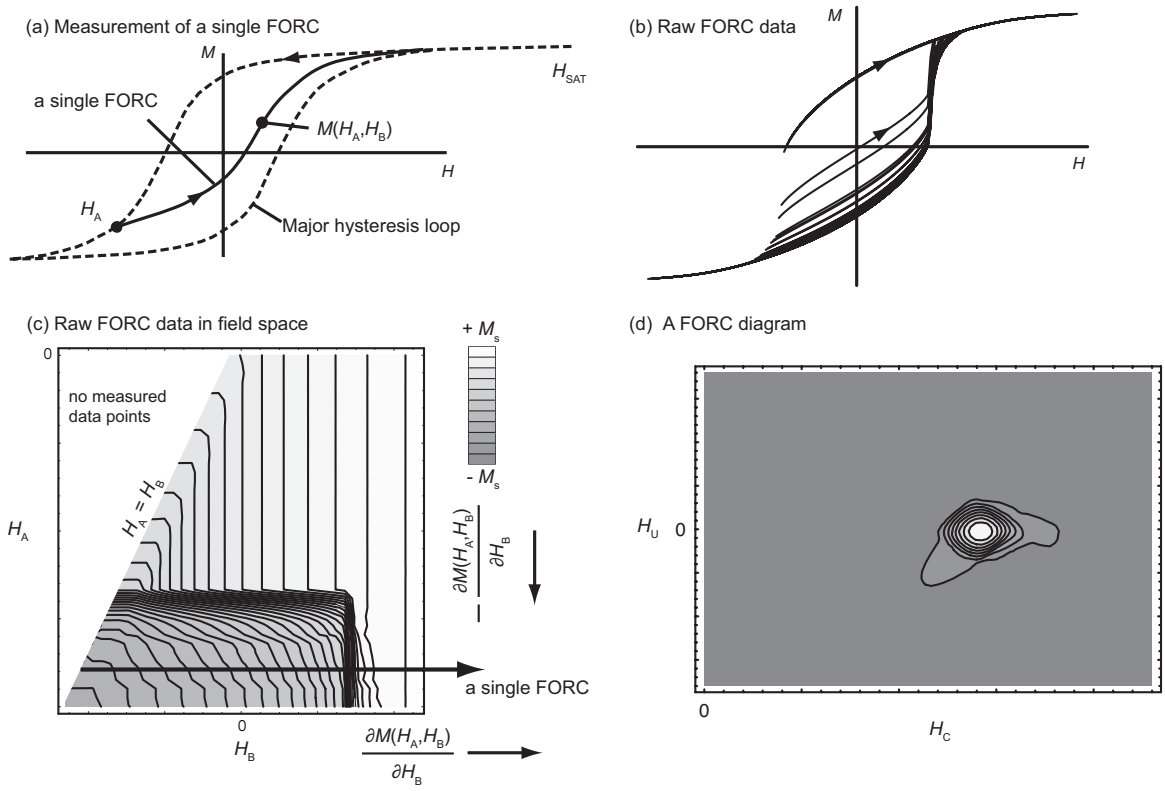
(a) Measurement of a single FORC
M
H
H_SAT
a single FORC
M(H_A,H_B)
H_A
Major hysteresis loop
(b) Raw FORC data
M
H
(c) Raw FORC data in field space
+ M_s
- M_s
0
no measured
data points
H_A = H_B
H_A
∂M(H_A,H_B)/∂H_B
a single FORC
0
H_B
∂M(H_A,H_B)/∂H_B
(d) A FORC diagram
H_U
0
0
H_C

Figure 1

(a) Major hysteresis loop for a SD grain

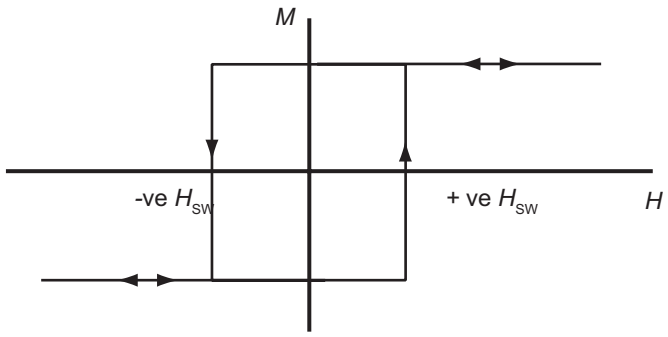

(b) Raw-data hysteresis data plotted in field-space

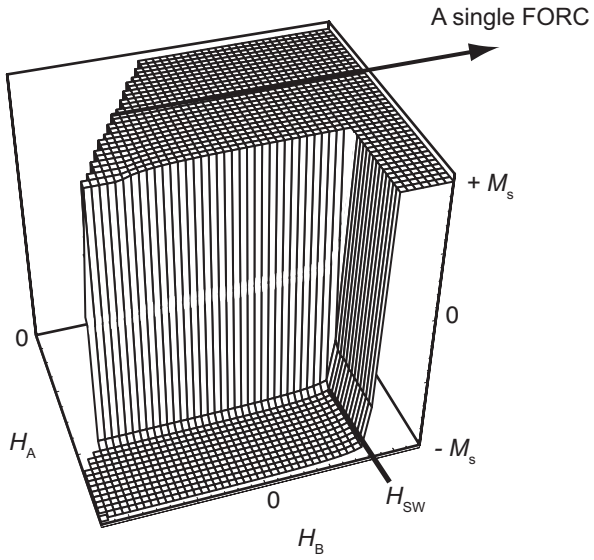

(c) FORC diagram for ideal SD grains

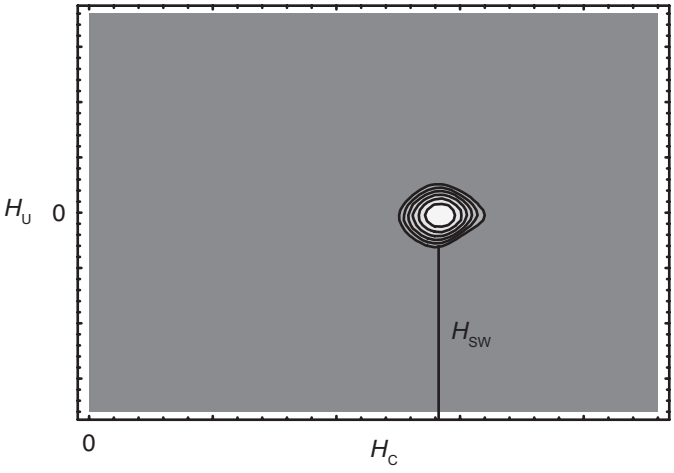

Figure 2

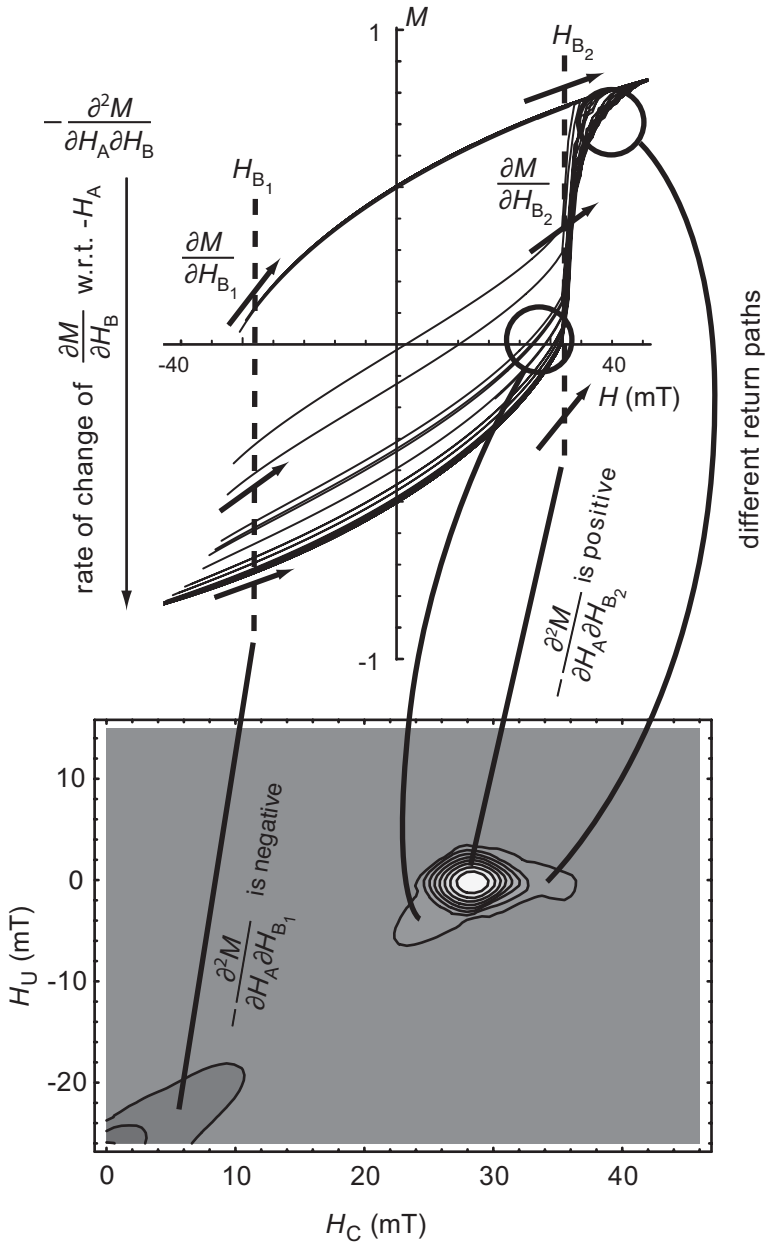

Figure 3

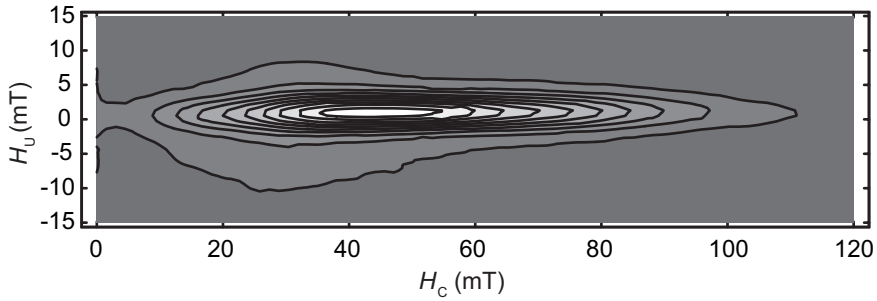

Figure 4

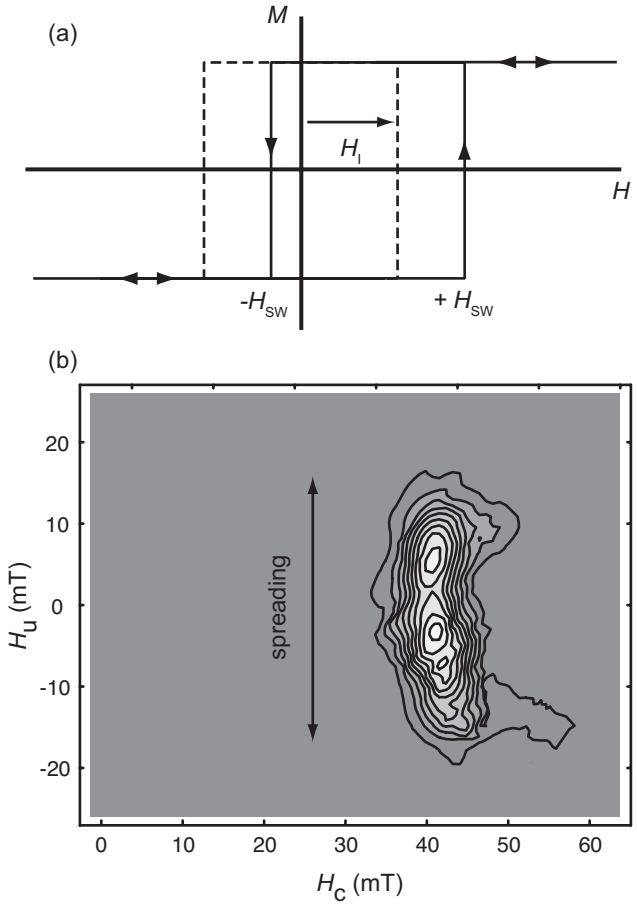

Figure 5

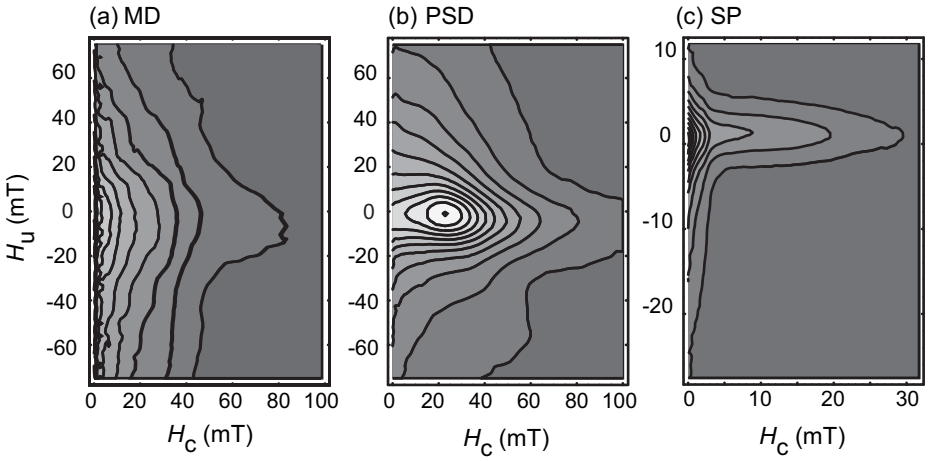

Figure 6

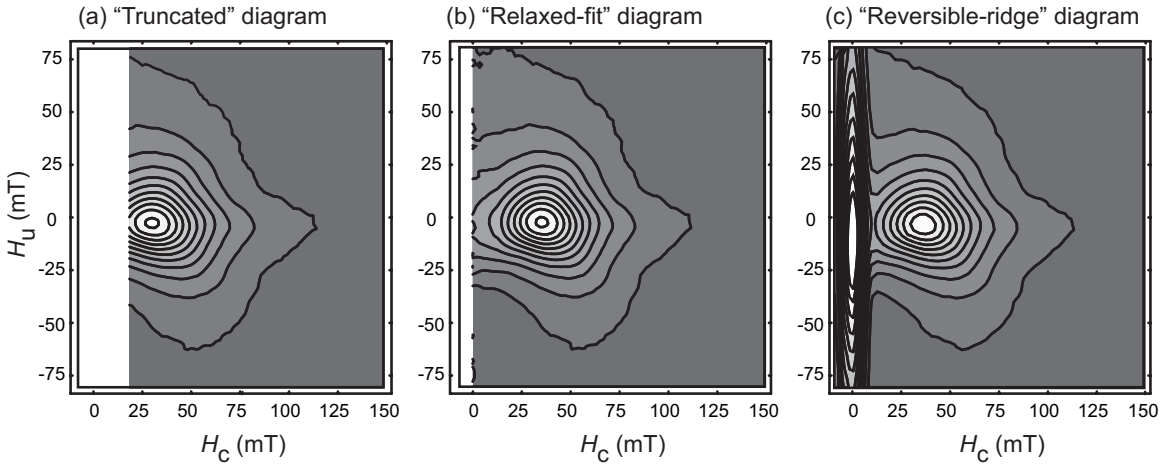

Figure 7

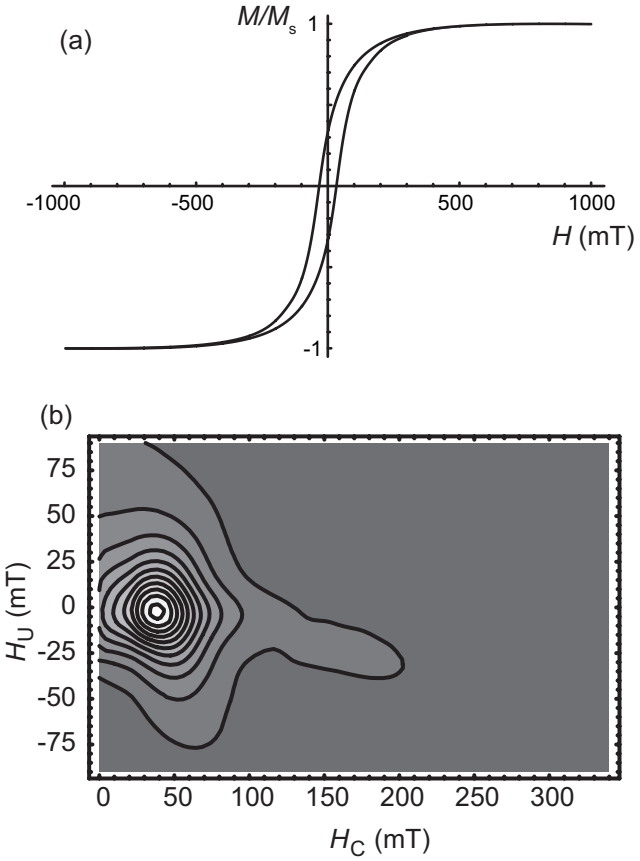

Figure 8